JOURNAL OF PROPULSION AND POWER
Vol. 17, No. 1, January–February 2001

Fuel Regression Rate in Hydroxyl-Terminated-Polybutadiene/Gaseous-Oxygen Hybrid Rocket Motors

Philmon George* and S. Krishnan†
Indian Institute of Technology Madras, Chennai 600 036, India
P. M. Varkey‡ and M. Ravindran§
Vikram Sarabhai Space Centre, Thiruvananthapuram 695 022, India
and
Lalitha Ramachandran¶
Liquid Propulsion System Centre, Thiruvananthapuram 695 547, India

The results of a systematic experimental investigation on the methods of enhancing the regression rate in hydroxyl-terminated polybutadiene (HTPB) fuel used in an HTPB/gaseous oxygen hybrid motor are presented. The effects of the addition of ammonium perchlorate (AP) or aluminum in the fuel, the variation of oxidizer–fuel ratio, and the variation of characteristic dimensions of fuel grain are presented. For the extents of the parametric variations considered, while the addition of AP and/or Al and the reduction of grain port diameter enhance the regression rate, the effect due to the latter is the most significant one. Furthermore, the regression rate increases along the axis, and it becomes essentially constant in the port region corresponding to a fuel-rich composition. The possible physical processes for all of these behaviors are discussed. The experimentally obtained exponents of the variables for regression rate (oxidizer mass flux and port diameter) are found to be significantly different from those of the conventional theory. The similarity between the fuel regression rate equation used in solid-fuel ramjet and that obtained in hybrid motor is discussed.

Nomenclature

A_t = nozzle throat area, m^2
B = mass transfer number
C_d = coefficient of discharge
c^* = characteristic velocity, m/s
c_c^* = characteristic velocity for fuel vaporized and oxygen injected, m/s
D = spatially averaged instantaneous port diameter, m
G = total mass flux, kg/m^2-s
G_o = spatially averaged instantaneous oxidizer mass flux, kg/m^2-s
L = fuel grain length, m
Le = Lewis number
m = mass, kg
$\dot{m}$ = mass flow rate, kg/s
Pr = Prandtl number
p = pressure, MPa
R = gas constant of oxygen, 259.8 J/(kg K)
$\dot{r}$ = regression rate, m/s
$\bar{\dot{r}}$ = spatially averaged instantaneous regression rate, m/s
$\tilde{\dot{r}}$ = spatially and temporally averaged regression rate, m/s
T = oxygen temperature, K
x = axial distance, m
γ = specific heat ratio of oxygen
Δt = time increment, s
η = combustion efficiency
μ = viscosity, kg/(ms)
ρ = fuel density, kg/m^3
Φ = oxidizer fuel mixture ratio

Subscripts

c = aft combustion-chamber
eff = effective
f = fuel
i = igniter, instant
o = oxidizer
s = sonic nozzle
t = total

Received 1 June 1998; revision received 11 November 1999; accepted for publication 20 January 2000.

*Research Scholar, Department of Aerospace Engineering; currently Information Technology Analyst, Tata Consultancy Services, Chennai 600 058, India.
†Professor of Aerospace Engineering and Head of Rocket and Missiles Laboratory; currently Visiting Professor, Faculty of Aerospace Engineering, Technion—Israel Institute of Technology, Haifa, Israel. Associate Fellow AIAA.
‡Scientist, Propellant Engineering Division.
§Scientist, Initiator and Igniter Division.
¶Deputy Project Director, Cryo Upper Stage Project.

Introduction

A ROCKET propulsion system in which one of the two propellant components (oxidizer or fuel) is in liquid phase and the other is in solid phase is a hybrid rocket motor. The combination of a solid fuel and a liquid oxidizer is the most common one.

The dependence of solid-fuel regression rate on various operating conditions is one of the most important design aspects in the study of hybrid motors. Marxman et al.,[1] Marxman,[2] and Marxman and Wooldridge[3] developed a turbulent boundary-layer regression-rate model based on the heat transfer mechanism. They assumed that the regression rate was controlled by the heat transfer mechanism to the fuel from the flame front that existed within the turbulent boundary layer. They used the Reynolds analogy and the approximation that $Le = Pr = 1$. Important results were that the regression rate is 1) a strong function of the total mass flux ($\dot{r} \propto G^{0.8}$), 2) independent of the pressures at motor operating conditions (the combustion being diffusion limited at high pressures), 3) a weak inverse function of the axial distance ($\dot{r} \propto x^{-0.2}$), and 4) a weak function of the properties of fuel and oxidizer (heat of reaction and heat of gasification, $\dot{r} \propto B^{0.23}$). The first two points were validated by the spatially and temporally averaged regression rate $\tilde{\dot{r}}$ results obtained (weighing the grains or measuring the grain dimensions before and after the tests).[1,4] A qualitative argument for the satisfaction of the third point was presented from their experimental results.[4] However, their

experimental program[1,4] did not address the validation of the fourth point. Furthermore, at lower pressures (<1.0 MPa), they observed experimentally the pressure dependence on regression rate: $\dot{r}$ decreased as pressure was decreased. This observation could not be captured by their basic heat transfer model[1–3]: They later argued that at lower pressures the regression rate could be dominated by the gas-phase chemical kinetics rather than the heat transfer mechanism.[3] The design aspects of hybrid motors are summarized in Ref. 5.

Smoot and Price[6–8] made significant contributions to the experimental data on hybrid-fuel regression rate essentially at low pressure conditions (≤1.2 MPa). They demonstrated the dependence of regression rate on oxidizer mass flux as well as pressure. The measurements at different pressures (0.24–1.2 MPa) and different oxidizer mass fluxes ($10 \le G_o \le 120$ kg/m^2-s) showed that 1) at low oxidizer mass fluxes (≤25 kg/m^2-s) the averaged regression rate $\tilde{\dot{r}}$ is G_o dependent ($\tilde{\dot{r}} \propto G_o^{0.8}$) but is pressure independent; 2) at high oxidizer mass fluxes (≥70 kg/m^2-s) it is G_o independent but is pressure dependent ($\tilde{\dot{r}}$ increases with p); and 3) at intermediate oxidizer mass fluxes, however, $\tilde{\dot{r}}$ is G_o dependent as well as pressure dependent. They attributed the pressure dependence to the rate limiting chemical kinetic processes, possibly heterogeneous in nature. Therefore, the classical turbulent boundary-layer regression-rate model based on heat transfer mechanism was extended to include the effects of condensed-phase surface products. Agreement was good for low oxidizer mass fluxes, but the extended model did not account for the observed pressure dependence for intermediate as well as high G_o.

Muzzy,[9] after discounting the possibility of rate limiting heterogeneous chemical kinetic processes at the gas–solid interface, considered the influence of chemical kinetic processes in gas phase that cannot be neglected for the conditions of low pressures and/or high total mass fluxes. He showed through calculations that, at low-pressure conditions, the regression rate was not that strong a function of total mass flux and was also dependent on pressure ($\dot{r} \propto G^{0.4} p^{0.5}$). Additionally, through experiments, he showed that the regression rate was essentially independent of the temperatures of the fuel grain and the oxidizer. Ramohalli and Stickler[10] developed a theory based on the differences in polymer degradation behaviors in inert and noninert environments to account for the pressure-dependent hybrid combustion. They argued that, under all conditions, a finite flux of unreacted oxidizer gas to fuel wall could exist through the mechanism of bulk turbulent eddy transport across the flame front. They concluded that the observed pressure dependence on regression rate at low pressure or high mass flux conditions could be due to the fuel wall oxidative (catalytic) depolymerization, which aids thermal degradation in producing vaporizable fragments.

Paul et al.[11] conducted experiments on a rubber/oxygen + nitrogen system and found that the exponent on B is 0.5 instead of 0.23, the value theoretically obtained by the authors of Refs. 1–3. Hence they,[11] after accounting for the density variation across the boundary layer, estimated the blocking effects, the effects of transpiration on skin-friction factor and heat transfer coefficient, and demonstrated that the regression rate was a strong function of B. Paul et al.[12] experimentally obtained the fuel regression rates in a hypergolic combination (difurfurylidene cyclo–hexanone + red fuming nitric acid) for different mass fluxes and pressures. The regression rate was found to be pressure independent above 1.0 MPa. The regression rate was calculated based on the curve fit of the integrated regression-rate expression $\dot{r} = aG_o^n$ or $\dot{r} = aG^n x^{n-1}$, where x the axial distance. They found that the exponent n of the regression-rate law was about 0.5 or a little lower and not 0.8 even though the flow through the port was turbulent. Later, Paul[13] found that the exponent n was less than 0.8, that is, $n = 0.6$, also in a nonhypergolic system of natural rubber + gaseous oxygen.

The growing interest in hybrid rocket propulsion has initiated many research programs in recent years.[14–23] Strand et al.[14] studied the solid-fuel regression rate in a hybrid-combustion model of a rigor higher than that of the classical turbulent boundary-layer model of the 1960s. They confirmed the turbulent boundary-layer heat transfer to be the rate limiting process for hybrid-fuel decomposition and combustion for motor-operating pressures. Strand et al.[14–16] also experimentally obtained oxidizer-mass-flux exponent n in the range from 0.56 (for $3 \le G_o \le 14$ kg/m^2-s) to 1 (for $7 \le G_o \le 70$ kg/m^2-s) for $\tilde{\dot{r}}$ in a hydroxyl-terminated polybutadiene (HTPB)/gaseous oxygen (GOX) system. Lewin et al.[17] through their experimental study in HTPB/GOX hybrid motors showed that the ballistically calculated spatially averaged instantaneous regression rate $\bar{\dot{r}}$ was G_o dependent and pressure independent over a G_o range of 11–400 kg/m^2-s and pressure range of 0.8–2.3 MPa. They found that the exponent n of the regression rate law $\bar{\dot{r}} = aG_o^n$ varies with fuel grain length, and it was 0.46 for longer fuel grains (203 mm) and 0.625 for shorter grains (89 mm). Chiaverini et al.,[18] from their experimental study on HTPB/GOX two-dimensional hybrid motors ($G_o \le 338$ kg/m^2 s, $1.3 \le p \le 9.0$ MPa), concluded that the instantaneous regression rate increased continuously in the axial direction. This was argued to be due to the increased total mass flux.

Thus we see that in hybrid motors the solid-fuel regression rate, a very important design parameter, is dependent on operating variables such as mass flux, pressure, properties of fuel and oxidizer, and fuel grain geometry. The classical turbulent boundary-layer regression-rate model based on heat transfer mechanism more or less explains the solid-fuel regression-rate behavior at high pressures relevant to motor-operating conditions. Accepting this basis for fuel regression-rate behavior, subsequent model studies[11,14] with enhanced rigor have confirmed the dependence. Though many experimental studies have confirmed the regression rate to be mass flux dependent and pressure independent, the mass flux exponents obtained through the real-time measurements, as well as the ballistic calculations using pressure–time data, point to a value significantly less than 0.8. The effect of the properties of fuel and oxidizer (affecting mass transfer number B) has been considered by Paul et al.[11] experimentally as well as theoretically and shown to be higher than the originally calculated value ($B^{0.23}$). No systematic experimental study has so far been reported on the effect of fuel grain geometry. Experimental data at motor operating mass flux conditions are lacking.

For hybrid motors, most of the presently projected fuel and oxidizer combinations in their basic form have fuel regression rate around 1.5 mm/s or less under motor-operating conditions. This low regression rate of solid fuel is the basic problem that degrades the application of hybrid motors. To address this issue, many studies have been conducted in recent years. Korting et al.[24] observed that a rearward-facing step could have a noticeable effect on combustion behavior, increasing the regression rate by changing the profile of the burned fuel grain. Strand et al.[14] supported the inclusion of particulate additives (aluminum and/or coal) in solid fuel as an approach to enhance fuel regression rate. Lewin et al.[17] showed that the fuel grains of shorter length (89 mm) had a higher regression rate than those of longer length (203 mm). Ramaholli et al.[19] claimed a 30% increase in regression rate of HTPB fuels with the use of a chemical bond-breaking catalyst.

In view of the preceding literature survey, the present study, with a primary goal of investigating the methods of regression-rate enhancement, reports the results of a systematic investigation conducted at high mass flux conditions. HTPB/GOX propellant combination was adopted for the study because it is of current interest in large booster applications. The comparative effects of the addition of ammonium perchlorate (AP) and/or aluminum powder in fuel composition, the oxidizer–fuel ratio, and the characteristic dimensions of fuel grain on fuel regression rate are presented. For the extents of parametric variations considered, the effect of the reduction of fuel grain port diameter is found to be the most significant one for the enhancement of regression rate.

Experimental Procedure

Test Facility

A high-pressure hybrid motor test facility is used. The oxygen supply is from a bank of cylinders kept at a maximum pressure of 15.0 MPa. A ball valve is used to initiate and terminate the flow of oxygen, and a sonic nozzle in the line maintains a desired constant mass flow rate. Nitrogen is used as a purge gas to terminate combustion after the desired burning time. The pressure maintained upstream of sonic nozzle is always kept higher than two times the maximum pressure of combustion chamber, so that the oxidizer-mass-flow rate is constant during the entire test. Oxygen supply to the motor (mounted on a thrust stand) is through two 20-mm flexible

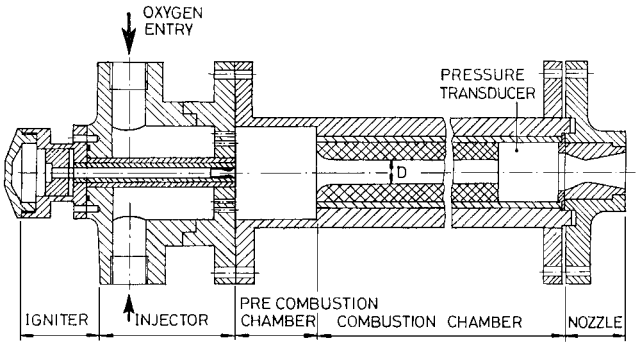

Fig. 1 Hybrid motor assembly.

Teflon® hoses. The high-pressure (4.0-MPa) axisymmetric hybrid motor assembly (Fig. 1) consists of an injector, a pyrogen igniter, a precombustion chamber, a combustion chamber with a fuel grain and an aft mixing chamber, and a nozzle assembly with interchangeable nozzles. The diameter and length of the precombustion chamber are 75 and 50 mm, respectively. The hybrid combustion chamber is a thick steel cylinder of outer diameter equal to 88.9 mm and inner diameter equal to 58.4 mm; combustion chambers of two different lengths (380 and 580 mm) are available.

The nozzle used for the first two tests were made of low-density graphite (density equal to 1600 kg/m^3). As excessive throat erosion was experienced during these tests, the low-density graphite nozzles were replaced with heavy copper nozzles. These copper nozzles could withstand a maximum firing duration of 8 s for unmetallized fuel grains. When metallized fuel grains were used, however, the copper nozzles started to melt beyond 3 s. Hence, for these grains high-density graphite (density equal to 1800 kg/m^3) nozzles were used; for these, the erosion rate on the radius was around 0.09 mm/s. For the first eight tests, igniters of 3-s duration were used. Because successful ignition could be obtained within 1 s, in subsequent tests the strong igniters of 3 s were successfully replaced with 1 s ones.

Fuel Specimen

The solid-fuel composition was mainly of HTPB. A small amount of carbon black (C) was mixed with the fuel. Trimethelol propane (TMP) was also added to improve the mechanical property of the grain; for curing toluene di-isocyanate (TDI) was used. The preparation of fuel grain was as follows. The premix containing HTPB, C, and TMP was thoroughly mixed for 10 min. Then after adding TDI, the blend was mixed for an additional 10 min. The percentage mass composition of the base fuel was HTPB:C:TMP:TDI = 81.68:0.82:4.08:13.42. The mixture was then poured into the mold of cylindrical fuel grain and cured, first for three days at room temperature and then for four days at 60°C. Four different fuel compositions were studied, as given in Table 1; these compositions will be referred by the names within the parentheses. The base fuel composition with or without the additives (AP and/or aluminum) was maintained as earlier. The particle size $[\Sigma(n_i d_i^4)/\Sigma(n_i d_i^3)]$ of the aluminum powder was 28 μm and that of AP was 98 μm. The details of grain geometry are also given in Table 1. The mechanical properties of these grains are given in Table 2.

Before fixing the fuel grain into the combustion chamber, the chamber inner wall was lined with two layers of 2-mm-thick nitrile-rubber-based insulator. Then the cured grain was bonded to the liner using epoxy. For the initial tests, however, silica phenolic liners were used; because of the problems faced in their fabrication, they were replaced with nitrile-rubber-based ones.

Test Schedules

The parameters varied for this study are also detailed in Table 1. For the present study, 43 tests, including 33 successful ones (15 successful sets), were carried out. A repeatable test was taken as successful. Initially three repeatable tests were taken for a successful set. When the confidence level improved, two successful tests were taken to be adequate.

Table 1 Experimental parameters

Parameter	Value
Fuel composition	
HTPB:C:TMP:TDI	81.63:0.82:4.08:13.47(HTPB grain)
HTPB:C:TMP:TDI:AP	75.47:0.76:3.77:12.457.55 (AP grain)
HTPB:C:TMP:TDI:Al	65.57:0.66:3.28:10.8219.67 (Al grain)
HTPB:C:TMP:TDI:AP:Al	61.54:0.62:3.08:10.156.15:18.46 (AP + Al grain)
Grain geometry,[a] mm (length × initial port diameter)	160 × 12 250 × 12 400 × 12 250 × 20 400 × 20 545 × 20
Initial steady-state pressure	2.0 MPa 3.0 MPa

[a]Fuel o.d. = 46.4 mm.

Table 2 Mechanical properties

Parameter	HTPB grain	AP grain	Al grain	AP + Al grain
Density, kg/m^3	960	1004	1120	1135
Tensile strength, MPa	1.87	1.97	2.11	2.18
Elongation, %	89	89	89	90
Stress at 50% elongation, MPa	1.26	1.43	1.47	1.77
Hardness Shore A	62	65	62	70

Each test run included the following steps. By suitable setting of the oxygen ball valve opening, a constant supply pressure of GOX was maintained upstream of the sonic nozzle. After the flow became steady, the igniter train was initiated. After the desired burn time, in quick successions oxygen supply was cut off and nitrogen purge was opened to extinguish combustion. The test measurements were the thrust and the pressures: upstream and downstream of sonic nozzle, at aft combustion chamber, and at pyrogen igniter. All of the signals from strain-gauge-type thrust and pressure transducers were recorded using a data acquisition system. The sampling rate was 200 samples/s. The other pre- and posttest measurements were the fuel density, the oxygen temperature (atmospheric temperature), the initial and final nozzle throat diameters, and the initial and final fuel grain masses and dimensions. For each test, the desired oxygen mass flow rate could be obtained by choosing an appropriate sonic nozzle throat and its upstream pressure. All of the tests were conducted with an initial oxidizer mass flux of around 500 kg/m^2 s.

Data Reduction

With respect to time, the measured values of the thrust and the pressures at the sonic nozzle upstream p_s, the igniter chamber p_i, and the aft combustion chamber p_c are available. Because the flow Mach numbers at these points of pressure measurements are very low (<0.1), the values are taken as the stagnation ones. The oxygen mass flow rate through sonic nozzle is given by

$$\dot{m}_o = \frac{C_{ds} p_s A_{ts}}{\sqrt{RT}/\Gamma} \tag{1}$$

where

$$\Gamma = \sqrt{\gamma}[2/(\gamma+1)]^{(\gamma+1)/2(\gamma-1)}$$

The igniter mass flow rate is given by

$$\dot{m}_i = \frac{C_{di} p_i A_{ti}}{c_i^*} \tag{2}$$

Here C_{ds} and C_{di} are the experimentally calibrated values. The total mass flow rate through the hybrid motor nozzle is given by

$$\dot{m}_t = p_c A_t \big/ c_{\text{eff}}^* \tag{3}$$

where c^*_{eff} is the effective characteristic velocity of the total combustion products of the igniter and hybrid combustion chamber and it is given by[25]

$$c^*_{\text{eff}} = \frac{c^*_i \dot{m}_i + \eta c^*_c \dot{m}_o [(\Phi + 1)/\Phi]}{\dot{m}_i + \dot{m}_o [(\Phi + 1)/\Phi]} \tag{4}$$

The fuel mass flow rate is given by

$$\dot{m}_f = \dot{m}_t - (\dot{m}_o + \dot{m}_i) \tag{5}$$

At each time step, $\dot{m}_o$ and $\dot{m}_i$ are calculated from Eqs. (1) and (2). To calculate ballistically the spatially averaged instantaneous regression rate $\bar{\dot{r}}$, port diameter, and oxidizer mass fluxes, the following scheme is adopted:

1) Assume a value for η.

2) Assume a value for Φ. At the instant t_i for the measured $p_{c,i}$ and the assumed value of Φ, calculate c^*_c using the complex chemical equilibrium code CEC71 (Ref. 26). Calculate c^*_{eff} from Eq. (4).

3) Calculate $\dot{m}_t$ using Eq. (3). Calculate $\dot{m}_f$ using Eq. (5). $\Phi' = \dot{m}_o/\dot{m}_{f,i}$.

4) Is $\Phi' = \Phi$? If not, go to step 2.

5) Calculate

$$\bar{\dot{r}}_i = \dot{m}_{f,i}/(\pi D_i L \rho) \tag{6}$$

$$G_i = \frac{\dot{m}_{t,i}}{(\pi/4) D_i^2} \tag{7}$$

$$G_{o,i} = \frac{\dot{m}_{o,i}}{(\pi/4) D_i^2} \tag{8}$$

6) Under the quasi-steady-state assumption, the spatially averaged port diameter at the next time step is given by

$$D_{i+1} = D_i + 2\bar{\dot{r}}_i \Delta t \tag{9}$$

7) Find

$$m'_{f,(i+1)} = m'_{f,i} + \dot{m}_{f,i} \Delta t \tag{10}$$

8) Calculate till extinguishment. The integrated total fuel mass consumed m'_f is compared with the measured one m_f, that is, the one obtained by weighing the fuel before and after the test. Is $m'_f = m_f$? If not, go to step 1.

The disadvantages of this method are that the calculation assumes 1) constant combustion efficiency throughout each test and 2) that the igniter combustion products do not participate in the hybrid motor combustion. The mass flow rate of the igniter combustion products is around 10% of total flow rate. Furthermore, it is already combusted matter. Therefore, the second part of the assumption is reasonable. The values of the converged combustion efficiencies obtained varied between 0.89 and 0.93. A logical variation in combustion efficiency could be observed between metallized and unmetallized grains: The metallized one had a combustion efficiency of 0.89, and the unmetallized one had a higher combustion efficiency around 0.93. The efficiency variation between a set of repeatable tests was mostly around 1% but always within 2%. The calculated spatially averaged port diameter at extinguishment and the measured spatially averaged port diameter of the burnt grain varied within 2%. Considering the errors involved in the measurement of pressures and temperature and the subsequent fuel mass flow rate calculation, the uncertainty in regression rate is found to be within ±3.5%.

Results and Discussion

As a typical test output, the combined pressure- and thrust-time record of test 43 is shown in Fig. 2. During the igniter operation, evidently due to the significant igniter mass flow contribution to the total flow, the chamber pressure is about 0.2 MPa higher than the equilibrium chamber pressure.

Oxidizer Mass Flux and Composition Effect

All of the tests for HTPB and AP grains were run at a constant pressure of 2.0 MPa using copper nozzles. The test for Al grains, however, could be run only under reducing pressure conditions (2.0–1.2 MPa) because of the erosion in the high-density graphite nozzle used. The spatially averaged instantaneous regression rates $\bar{\dot{r}}$ vs oxidizer mass fluxes for the HTPB and Al grains (Table 1) are shown in Fig. 3. The oxidizer mass flux exponent n in the regression rate equation $\bar{\dot{r}} = aG_o^n$ is 0.53 for HTPB grain and 0.93 for Al grain. For the same grain dimensions, Fig. 4 shows the regression rates of HTPB grains and AP grains. The oxidizer mass flux exponent n is 0.71 for AP grain. Whereas these results in Figs. 3 and 4 are for the grain dimension of 250 × 12 mm, the trend

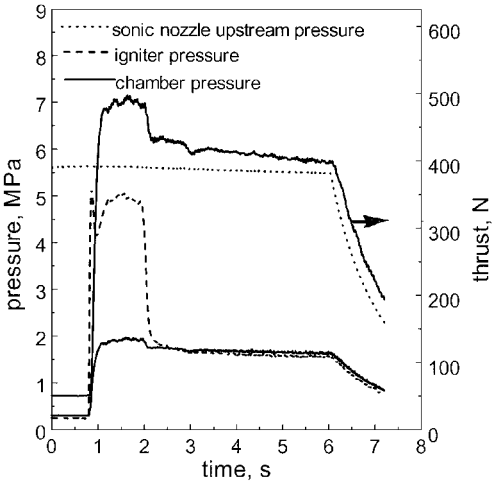

Fig. 2 Pressure- and thrust-time traces of hybrid motor testing.

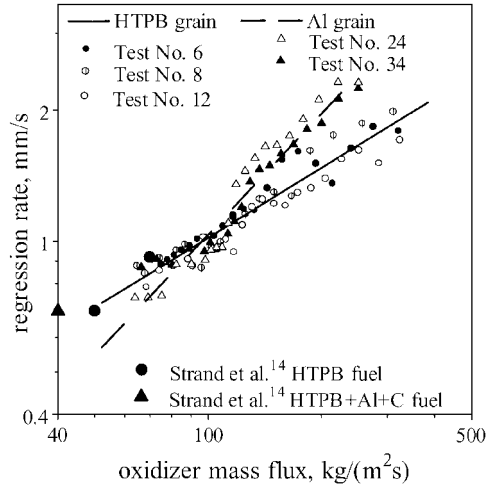

Fig. 3 Regression rates of HTPB and Al grains: grain length × initial port diameter = 250 × 12 mm.

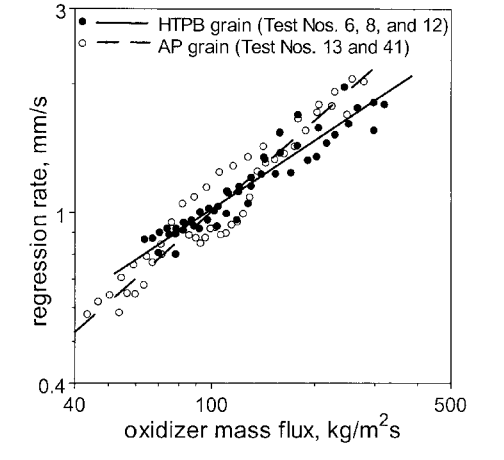

Fig. 4 Regression rates of HTPB and AP grains: grain length × initial port diameter = 250 × 12 mm.

Table 3 Spatially averaged instantaneous regression rate $\dot{r}$ equations at 2.0 MPa

Grains	Grain I, 250 × 12 mm	Grain II, 400 × 20 mm	Grains I and II
HTPB	$8.7 \times 10^{-5} G_o^{0.53}$	$7.7 \times 10^{-5} G_o^{0.53}$	$6.37 \times 10^{-5}\ G_o^{0.41} D^{-0.24}$
Al[a]	$1.4 \times 10^{-5} G_o^{0.93}$	$1.3 \times 10^{-5} G_o^{0.89}$	——
AP	$3.8 \times 10^{-5} G_o^{0.71}$	$2.8 \times 10^{-5} G_o^{0.72}$	$1.88 \times 10^{-5} G_o^{0.42} D^{-0.60}$
AP + Al[a]	$1.2 \times 10^{-5}\ G_o^{0.97}$	——[b]	——

[a]There was pressure reduction due to nozzle erosion. [b]Not investigated.

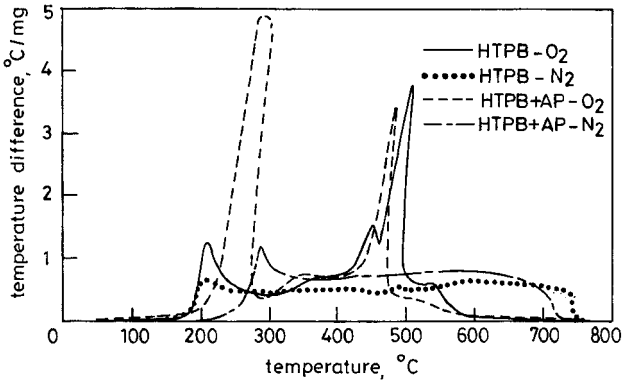

Fig. 5 DTA traces of the samples of HTPB and AP grains in oxygen and nitrogen atmosphere.

is repeatable for the grain dimension of 400 × 20 mm as given in Table 3.

The enhancement of regression rate due to aluminum addition has been known for a long time.[4] Aluminum was originally added for an increase in specific impulse and a 20–30% increase in regression rate was also observed. Because aluminum is ejected without vaporizing, this increase in regression rate checks out with a simple thermal balance calculation where one takes into account the decrease in effective heat of vaporization. At 1.6 MPa, in the range of oxygen mass flux 30–80 kg/m^2-s, Wooldridge et al.[4] found that the regression rate of polybutadiene–acrylic–nitrile and polyurethane grains could be enhanced by 26% by the addition of 20% aluminum. At 1.3- and 1.5-MPa pressure conditions, in the range of oxygen flux 10–50 kg/m^2-s, by modeling and experimental studies Strand et al.[14] found that the regression rate of HTPB grains could be enhanced by 17% by the addition of aluminum. Their HTPB grains contained particulates of 40% aluminum and 30% carbon. On the mechanism of regression rate enhancement by aluminum addition, they argued that the augmented radiative heat transfer was the cause. They further demonstrated theoretically as well as experimentally that, the radiation being pressure dependent, the regression-rate enhancement due to aluminum addition should also be pressure dependent. Their results for the HTPB (1.3–1.5 MPa) and the particulated HTPB grains (1.5 MPa) are also shown in Fig. 3. Their results for the HTPB grains are comparable to the results of the present study. Their regression rate of the particulated grain, however, is significantly higher than the present result. There could be two likely reasons: 1) the higher particulate content and 2) the higher pressure; both because a higher radiative heat transfer component would lead to a higher regression rate. Again, because radiative heat transfer is pressure dependent, the actual G_o exponent at a fixed pressure of 2 MPa is expected to be less than the value of 0.93 found in the present study for a reducing pressure conditions from 2 to 1.2 MPa.

The differential thermal analyzer (DTA) traces for the samples of the HTPB grain and the AP grain with purges of oxygen and of nitrogen at 1-atm pressure are given in Fig. 5. With a nitrogen purge, an exothermic peak is observed around 200°C for the HTPB grain; in the case of the AP grain, the peak is found to be delayed around 280°C with a slightly higher exothermicity. With an oxygen purge, a similar peak but of higher exothermicity is observed around the same 200°C for the HTPB grain; furthermore, comparably in the case of the AP grain a similar delayed peak but of substantially enhanced exothermicity is found around 240°C. These DTA observations have corresponding records in the experiments with a thermogravimetric analyzer (TGA). In fact, with the oxygen purge one could hear the sound of an explosion at 240°C in the case of TGA experiment for the sample of the AP grain

When the exothermicity at low temperatures (200–300°C) for the sample of the AP grain with a nitrogen purge is compared to that with an oxygen purge, exothermicity with the latter is found to be substantially enhanced. Because the AP content in the AP grain is only 7.55% apart, suspecting that this enhanced exothermicity could be because of the reaction between the evolved ammonia from AP and the oxygen, a DTA experiment with an oxygen purge for AP crystal was conducted. With an inert purge at 1-atm pressure, AP crystal is known to change its crystalline lattice from orthorombic to cubic at 240°C with a sharp endothermic peak and to decompose very rapidly and explode at 460°C (Ref. 27). Interestingly the DTA and TGA traces with an oxygen purge obtained in the present study are not different from the respective traces with a nitrogen purge. Furthermore, the absence of any appreciable enhancement in the exothermicity between the samples of HTPB grain and AP grain under nitrogen purge discounts the possibility of heterogeneous/gas-phase reaction among fuel/fuel vapor, perchloric acid, and ammonia. Then, the reason for the substantially enhanced exothermicity with an oxygen purge in the samples of the AP grain could be the following. In the presence of the AP decomposed products, namely, ammonia and perchloric acid, the thermally decomposed fuel vapor and the purge oxygen are able to react more violently at low temperatures due to significantly different gas-phase kinetics.

Although this is the situation for thermal analysis experiments, the application of these results for hybrid motor operating conditions should be considered. In the grain port, the decomposed fuel vapor and the AP decomposition products from the fuel surface convect toward the flame front, which is expected to be at a distance of about 10% of the port radius under fully developed turbulent flow conditions.[28] As the flame front temperature is not going to be significantly different by the addition of small quantity of AP, if any regression-rate enhancement is to take place by the addition of AP, there should be a supplementary heat source other than the flame front. This is possible only when oxygen is available closer to the fuel surface in which region the decomposed fuel vapor and the AP decomposition products are convecting toward the flame front. Conceivably, a finite flux of oxygen to fuel surface could exist through the mechanism of bulk turbulent eddy transport across the flame front at higher mass flux conditions.[10] Therefore, the addition of AP is able to enhance the regression rate at high mass flux conditions but not under low mass flux conditions, as shown in Fig. 4. However, the exact physical and chemical processes under which the substantially enhanced exothermicity occurs for the samples of AP grain with oxygen purge in DTA experiments cannot be expected to happen in rocket operating conditions because in the latter the heating rates are about four order of magnitude and the pressures are more than one order of magnitude higher than those in thermal analyzers.

Pressure Effect

The spatially averaged instantaneous regression rates vs oxidizer mass fluxes for the 20-mm AP grains at 2.0 and 3.0 MPa are shown in Fig. 6. These results indicate that the pressure does not have much effect on regression rate. Similar results are obtained for the 20-mm HTPB grain at 2.0 and 3.0 MPa. These results are in agreement with the results of earlier studies of Wooldridge et al.[4] and Paul et al.[11] at high pressures (>1.0 MPa). However, the pressure independency is not that well marked for 12-mm grains.

Length Effect

Initially for a few tests the port entry was sharp (not well rounded). In these cases a high regression rate was observed locally at a few millimeters downstream of the port entry. This was rationalized to be due to a separation and reattachment of the entry flow. With the flame front established at the vicinity of the reattachment point, the

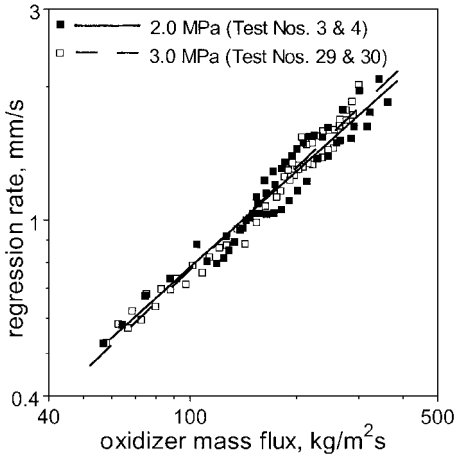

Fig. 6 Regression rates of AP grains at 2.0 and 3.0 MPa: grain length × initial port diameter = 400 × 20 mm.

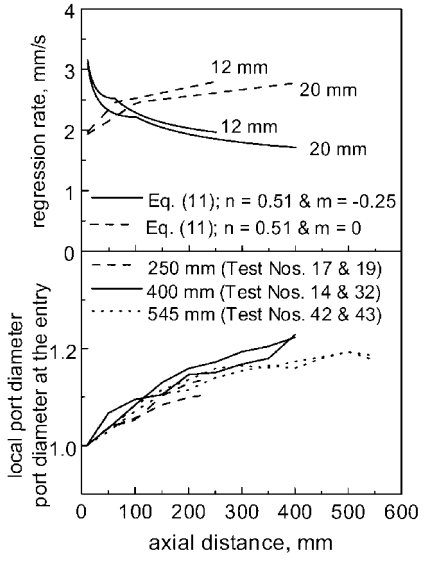

Fig. 7 Regression rate variation per $r \propto G^n x^m$ for grains of initial port diameters of 12 and 20 mm (top). Ratio of the experimental local diameter to the entry diameter for HTPB grains of initial port diameter = 20 mm (bottom).

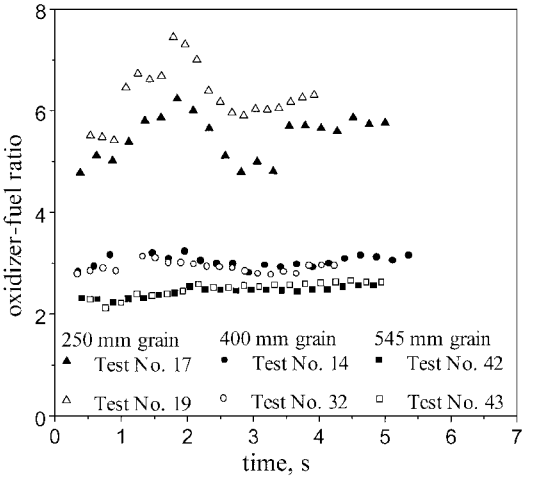

Fig. 8 Oxidizer–fuel ratio with respect to time for HTPB grains: initial port diameter = 20 mm.

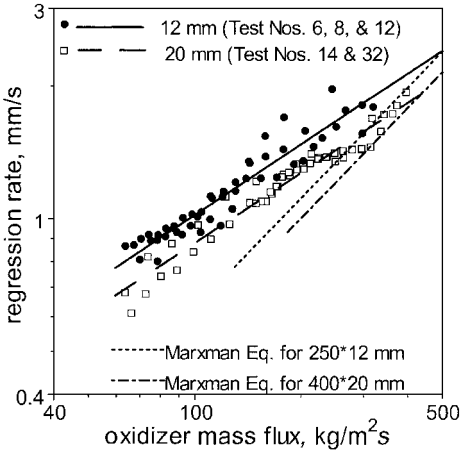

Fig. 9 Regression rates of HTPB grains: grain length × initial port diameter = 250 × 12 and 400 × 20 mm.

local regression at that point was high. Subsequently all of the fuel grains were given well rounded port entries. From the measurements of web thickness after each test, the local port diameter is found to increase along the axis. This is because the regression rate is a function of local mass flux and the local mass flux increases along the axis. In the bottom of Fig. 7, the ratio of the local port diameter to the entry port diameter for HTPB grains of initial port diameter of 20 mm and three different lengths (250, 400, and 545 mm) are presented. It can be seen that for 545-mm grain, the increase in local port diameter diminishes toward the aft end of the grain indicating a reduced regression rate after 400 mm.

The variations of oxidizer–fuel ratio with respect to time for the HTPB grains are shown in Fig. 8. Here it is seen that the 400 × 20 mm grains operate closer to the stoichiometric oxidizer–fuel ratio (2.95). However, the 250 × 20 mm grains operate at a fuel-lean condition and the 545 × 20 mm grains operate at a fuel-rich condition. The high dispersion in the oxidizer–fuel ratios for the tests of the 250-mm grain is because of the combustion pressure oscillations experienced. At a fuel-rich condition, theoretically, the stoichiometric diffusion flame can be expected to be present only up to the grain length where the oxygen is available. Thereafter the hot combustion gases would flow in the absence of the diffusion flame but with the continued addition of vaporized fuel from grain. This fuel addition could reduce the core gas temperature resulting in reduced temperature difference between the core gas and the wall. However, the mass flux would continue to increase along the axis. Therefore, the reduced regression rate for 545 × 20 mm grain after 400 mm could be due to the net reduction in heat transfer under the two opposing situations described.

Diameter Effect

The regression rates of HTPB grains with two different initial port diameters are shown in Fig. 9. The values of a and n in the regression rate equation $\dot{r} = aG_o^n$ are given in Table 3. At a given oxidizer mass flux, the grain with the lower initial port diameter (12 mm) regresses faster than the one with the larger initial port diameter (20 mm). The regression rates obtained against the oxidizer mass fluxes have the port diameters varying from 12 to 40 mm. From the present data, to distinguish the effect of port diameter as well as G_o on $\dot{r}$, equations are obtained by a suitable method for HTPB and AP grains and are given in Table 3. The obtained equation for the HTPB grain and the experimental data are presented in Fig. 10. The regression rate correlations with G_o and D given in Table 3 and Fig. 10 have been obtained for a maximum oxidizer mass flux of 500 kg/(m^2 s) and the port-diameter variation of 12–40 mm. Whereas the oxidizer-mass-flux range adopted in the present study approximately represents the large motor-operating conditions, the port-diameter variations do not. However, the correlations may give an indication of the size effect.

By the use of their turbulent boundary-layer regression-rate model based on the heat transfer mechanism the authors of Refs. 1–3

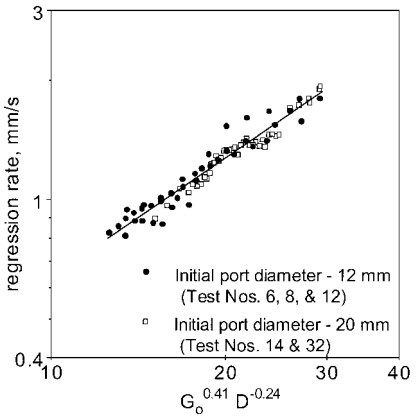

Fig. 10 Regression rate dependence on oxidizer mass flux and port diameter for HTPB grains.

obtained the well-known regression-rate mass flux equation. This Marxman equation, under the conditions of negligible radiant heat transfer, high operating pressures, and fixed oxidizer–fuel combination, can be written as

$$\dot{r} \propto G^n (x/\mu)^m \tag{11}$$

where $n = 0.8$ and $m = -0.2$. Here G is the local mass flux given by

$$G = \frac{\dot{m}_o + \dot{m}_f}{(\pi/4)(D - 2\delta^*)^2} \tag{12}$$

where δ^* is the boundary-layer displacement thickness given by[4,5]

$$2\delta^* = \begin{cases} 0.21D(x/x_A)^{0.8} & x \le x_A = 5D \\ 0.21D & x > x_A \end{cases}$$

Sometimes it is wrongly argued that the Marxman equation does not account for the effect of D on regression rate. If two grains of different port diameters are considered with the same oxidizer mass flux at the port entry, however, the one with a smaller diameter will have a higher gradient of total mass flux along the axis and, hence, will have a higher spatially averaged regression rate. Therefore, the Marxman equation predicts that the regression rate will decrease with 1) the decrease in mass flux, 2) the increase in port diameter, and 3) the increase in axial distance. The first two predictions are in qualitative agreement with the experimental observations. In the third case, most of the experimental studies, including the present study, show an increase[18] or constant regression rate along the axis. With reference to the regression-rate dependence on the mass flux and the port diameter, the values of the exponents in the regression-rate equation do not agree with many experimental findings. For engineering evaluations, several investigators plotted the experimental regression rate as a function of oxidizer mass flux. The exponents obtained were less than 0.8 and near 0.5. As early as 1965, Marxman and Wooldridge responded to this observation by stating that the correlations based on the total mass flux G would lead to an exponent $\cong$0.8, whereas those based on oxidizer mass flux G_o would only lead an exponent $\cong$0.5.[3] However, this argument seems to be not valid. The initial regression rate experimentally obtained in the present study for 12-mm HTPB grain at 500 kg/m^2 s oxidizer mass flux is taken as reference. The regression rates with respect to time for varying G_o were calculated through the conventional incremental analysis[29] using Eq. (11) for initial port diameters of 12 and 20 mm and are shown in Fig. 9. Here the value of n for G_o is more than 0.8. Furthermore the prediction for the diameter effect is only qualitative.

Now retaining the basic form of Eq. (11), the suitable values of n and m to match the experimental results of diameter effect shown in Fig. 9 can be found to be 0.51 and -0.25, respectively. Contrary to the observation of most of the experimental studies including the present one, however, these values of n and m continue to show a decrease in regression rate with the increase in axial distance (top Fig. 7). This unrealistic decrease in the regression rate with the increase in axial distance notwithstanding, the resulting higher spatially averaged regression rate for the smaller diameter and shorter length grain is only responsible for giving this pseudomatch (top Fig. 7). Furthermore, it is possible to find suitable new values of n and m to match the experimental results of increase in regression rate with axial distance, for example, $n = 0.51$ and $m \ge 0$ (Fig. 7). These new values, however, fail to predict the decrease in spatially average regression rate with the increase in port diameter because the spatially averaged regression rates for both the grains are essentially same.

Among the effects of AP addition, Al addition, and port diameter reduction, for the extents varied, the diameter effect is the most significant. In the design of hybrid rocket motor, the selection of grain-port diameter is dictated by ballistics requirements. However, in view of the higher regression rate feasible with a lower port diameter, the designer may look for the possibility of having a multiperforated grain instead of a single-perforated one. The multiperforated grain, due to the enhanced regression rate and possibly increased burning area, may result in reduced length-to-diameter ratio of the motor.

A large number of studies on combustion-chamber configuration similar to that of a hybrid motor have been conducted in recent years for solid-fuel ramjet (SFRJ).[30–32] Although the combustion processes in SFRJ are similar to those of hybrid motors, there are two major differences. First, the SFRJ employs air rather than a pure oxidizer; second, it has a sudden expansion of gaseous inlet flow. Because of this sudden expansion, three distinct flowfields exist: 1) recirculation zone, 2) reattachment region, and 3) zone downstream of reattachment. The zone downstream of reattachment in an SFRJ is very similar to the fully developed turbulent boundary-layer region in a hybrid motor. For SFRJs with large L/D ratios, the spatially averaged instantaneous regression rate will be controlled by the heat transfer mechanism to the fuel from the flame front that exists within the fully developed turbulent boundary-layer region. In such cases it is a common practice to obtain experimentally the spatially averaged instantaneous regression rate as a function of air mass flux and port diameter. Their exponents are found to be from around 0.4 to 0.6 and -0.25 to -0.4, respectively.[30] Similar exponents are obtained in hybrid motors (Table 3).

Combined Regression-Rate Enhancement

The primary motivation of the present study is to find through a systematic investigation the methods for the regression-rate enhancement. Therefore, the combined effect of the addition of AP and Al in the fuel and the port diameter are shown in Fig. 11. It is seen that the regression at the oxidizer mass flux of 300 kg/m^2-s

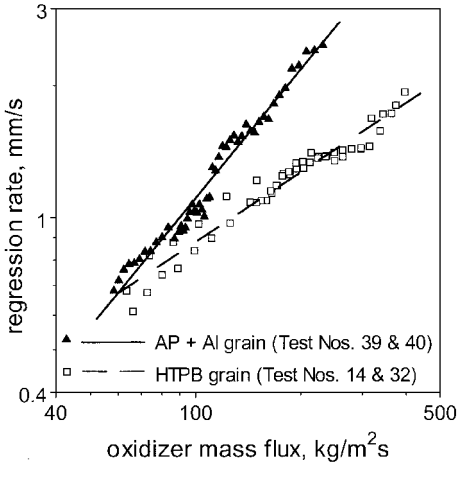

Fig. 11 Regression rates of HTPB grains with initial port diameter = 20 mm and AP + Al grains with initial port diameter = 12 mm.

can be enhanced by more than 100%, and this can be still higher at higher mass flux conditions.

Conclusions

1) The addition of AP and/or Al in HTPB fuel and the reduction of grain port diameter enhance the fuel regression rate in HTPB/GOX hybrid motors. The effect due to the latter is the most significant one for the extents of the parametric variations considered.

2) The addition of AP is able to enhance the regression rate at high mass flux conditions. Conceivably, this is because of an additional heat source available near the fuel surface. This heat source results from the reaction of the fuel vapor, the AP decomposition products, and the finite flux of oxygen to fuel surface. This oxygen flux exists through the mechanism of bulk turbulent eddy transport across the flame front at higher mass flux conditions.

3) With reference to the conventional theory, the regression rate decreases along the axis and it depends on the mass flux $G^{0.8}$. The present experimental results indicate that the regression rate increases along the axis and that the exponent of the mass flux is significantly less than 0.8.

4) Similarity exists between the fuel regression-rate equation used in an SFRJ and that obtained in a hybrid motor. In hybrid motors, the present study points to an equation for HTPB fuel as $\bar{\dot{r}} = 6.37 \times 10^{-5}\, G_o^{0.41} D^{-0.24}$ m/s and for HTPB + AP fuel as $\bar{\dot{r}} = 1.88 \times 10^{-5}\, G_o^{0.42} D^{-0.60}$ m/s.

Acknowledgments

The study reported forms a part of the research sponsored by the Space Technology Cell formed by the Indian Space Research Organization at the Indian Institute of Technology Madras. The first two authors had many useful discussions with S. R. Chakravarthy while writing this paper.

References

[1]Marxman, G. A., Wooldridge, C. E., and Muzzy, R. J., "Fundamentals of Hybrid Boundary Layer Combustion," *Heterogeneous Combustion*, edited by H. G. Wolfhard, I. Glassman, and L. Green Jr., Vol. 15, Progress in Astronautics and Aeronautics, Academic Press, New York, 1964, pp. 485–522.

[2]Marxman, G. A., "Boundary Layer Combustion in Propulsion," *Proceedings of the Eleventh (International) Symposium on Combustion*, Combustion Inst., Pittsburgh, PA, 1967, pp. 269–289.

[3]Marxman, G. A., and Wooldridge, C. E., "Research on the Combustion Mechanism of Hybrid Rockets," *Advances in Tactical Rocket Propulsion*, edited by S. S. Penner, CP-1, AGARD, Technivision Services, Maidenhead, England, U.K., 1968, pp. 421–477.

[4]Wooldridge, C. E., Marxman, G. A., and Kier, R. J., "Investigation of Combustion Instability in Hybrid Rockets," Final Rept., NASA CR-66812, Stanford Research Inst., Menlo Park, CA, 1969.

[5]Wooldridge, C. E., and Muzzy, R. J., "Internal Ballistic Considerations in Hybrid Rocket Design," *Journal of Spacecraft and Rockets*, Vol. 4, No. 2, 1967, pp. 255–262.

[6]Smoot, L. D., and Price, C. F., "Regression Rates of Nonmetallized Hybrid Fuel Systems," *AIAA Journal*, Vol. 3, No. 8, 1965, pp. 1408–1413.

[7]Smoot, L. D., and Price, C. F., "Regression Rates of Metallized Hybrid Fuel Systems," *AIAA Journal*, Vol. 4, No. 5, 1966, pp. 910–915.

[8]Smoot, L. D., and Price, C. F., "Pressure Dependence of Hybrid Fuel Regression Rates," *AIAA Journal*, Vol. 5, No. 1, 1967, pp. 102–106.

[9]Muzzy, R. J., "Applied Hybrid Combustion Theory," AIAA Paper 72-1143, 1972.

[10]Ramohalli, K., and Stickler, D. B., "Polymer-Degradation Theory of Pressure-Sensitive Hybrid Combustion," *Proceedings of the Thirteenth (International) Symposium on Combustion*, Combustion Inst., Pittsburgh, PA, 1971, pp. 1059–1077.

[11]Paul, P. J., Mukunda, H. S., and Jain, V. K., "Regression Rates in Boundary Layer Combustion," *Proceedings of the Nineteenth (International) Symposium on Combustion*, Combustion Inst., Pittsburgh, PA, 1982, pp. 717–729.

[12]Paul, P. J., Mukunda, H. S., Narahari, H. K., Venkataraman, R., and Jain, V. K., "Regression Rate Studies in Hypergolic System," *Combustion Science and Technology*, Vol. 26, No. 1, 1981, pp. 17–24.

[13]Paul, P. J., "Regression Rate and Low Frequency Instability Studies in Hybrid Rocket Engines," Ph.D. Dissertation, Dept. of Aerospace Engineerng, Indian Inst. of Science, Bangalore, India, 1982.

[14]Strand, L. D., Ray, R. L., and Cohen, N. S., "Hybrid Rocket Combustion Study," AIAA Paper 93-2412, June 1993.

[15]Strand, L. D., Jones, M. D., Ray, R. L., and Cohen, N. S., "Characterization of Hybrid Rocket Internal Heat Flux and HTPB Fuel Pyrolysis," AIAA Paper 94-2876, June 1994.

[16]Strand, L. D., Ray, R. L., Anderson, F. A., and Cohen, N. S., "Hybrid Rocket Fuel Combustion and Regression Rate Study," AIAA Paper 92-3302, July 1992.

[17]Lewin, A., Dennis, J., Conley, B., and Suzuki, D., "Experimental Determination of Performance Parameters for a Polybutadiene/Oxygen Hybrid Rocket," AIAA Paper 92-3590, July 1992.

[18]Chiaverini, M. J., Harting, G. C., Lu, Y., Kuo, K. K., Serin, N., and Johnson, D. K., "Fuel Decomposition and Boundary-Layer Combustion Processes of Hybrid Rocket Motors," AIAA Paper 95-2686, July 1995.

[19]Ramohalli, K., Bates, R., Jones, M., Wygle, B., and Yi, J., "Some Recent Results from a Program in Hybrids at the University of Arizona," AIAA Paper 95-2945, July 1995.

[20]Boardman, T. A., Carpenter, R. L., Goldberg, B. E., and Shaeffer, C. W., "Development and Testing of 11- and 24-Inch Hybrid Motors Under the Joint Government/Industry IR&D Program," AIAA Paper 93-2552, June 1993.

[21]Rice, T., and Akin, D. L., "Parametric Testing for Determination of Hybrid Rocket Engine Performance," AIAA Paper 94-3017, June 1994.

[22]George, P., Krishnan, S., Ramachandran, L., Varkey, P. M., and Ravindran, M., "Regression Rate Study in HTPB/GOX Hybrid Rocket Motors," *Defence Science Journal*, Vol. 46, No. 5, 1996, pp. 337–345.

[23]Gany, A., "Scale Effects in Hybrid Motors Under Similarity Conditions," AIAA Paper 96-2846, July 1996.

[24]Korting, P. A. O. G., Schoyer, H. F. R., and Timnat, Y. M., "Advanced Hybrid Rocket Motor Experiments," *Acta Astronautica*, Vol. 15, No. 2, 1987, pp. 91–104.

[25]Adams, D. M., "Igniter Performance in Solid-Propellant Rocket Motors," *Journal of Spacecraft and Rockets*, Vol. 4, No. 8, 1967, pp. 1024–1029.

[26]Gordon, S., and McBride, B. J., "Computer Program for Calculation of Complex Chemical Equilibrium Compositions, Rocket Performance, Incident and Reflected Shocks, and Chapman–Jauguet Detonations," NASA SP-273, 1971.

[27]Waesche, R. H. W., Wenograd, J., and Feinaner, L. R., "Investigations of Solid Propellant Decomposition Characteristics and Their Relation to the Observed Burning Rates," *ICRPG/AIAA IInd Solid Propulsion Conference*, Preprint, 1967.

[28]Schulte, G., Pein, R., and Hogl, A., "Temperature and Concentration Measurements in a Solid Fuel Ramjet Combustor Chamber," *Journal of Propulsion and Power*, Vol. 3, No.2, 1987, pp. 114–120.

[29]Miller, W. H., and Barrington, D. K., "A Review of Contemporary Solid Rocket Motor Performance Prediction Techniques," *Journal of Spacecraft and Rockets*, Vol. 7, No. 3, 1970, pp. 225–237.

[30]Krishnan, S., and George, P., "Solid Fuel Ramjet Combustor Design," *Progress in Aerospace Sciences*, Vol. 34, No. 3/4, 1998, pp. 219–256.

[31]Schulte, G., "Fuel Regression and Flame Stabilization Studies of Solid Fuel Ramjets," *Journal of Propulsion and Power*, Vol. 2, No. 4, 1986, pp. 301–304.

[32]Zvuloni, R., Gany, A., and Levy, Y., "Geometric Effects on the Combustion in Solid Fuel Ramjets," *Journal of Propulsion and Power*, Vol. 5, No.1, 1989, pp. 32–37.